Crystal-field states of UO_2 probed by directional dependence of nonresonant inelastic x-ray scattering

M. Sundermann,[1,2] G. van der Laan,[3,*] A. Severing,[1,2] L. Simonelli,[4,†] G. H. Lander,[5] M. W. Haverkort,[6] and R. Caciuffo[5]

[1]*Institute of Physics II, University of Cologne, Zülpicher Straße 77, D-50937 Cologne, Germany*
[2]*Max-Planck-Institute for Chemical Physics of Solids, Nöthnizer Straße 40, 01187 Dresden, Germany*
[3]*Magnetic Spectroscopy Group, Diamond Light Source, Didcot OX11 0DE, United Kingdom*
[4]*European Synchrotron Radiation Facility (ESRF), Boîte Postale 220, 38043 Grenoble Cédex, France*
[5]*European Commission, Joint Research Centre (JRC), Directorate for Nuclear Safety and Security, Postfach 2340, D-76125 Karlsruhe, Germany*
[6]*Institute for Theoretical Physics, Heidelberg University, Philosophenweg 19, 69120 Heidelberg, Germany*

(Received 1 July 2018; published 5 November 2018)

Nonresonant inelastic x-ray scattering (NIXS) has been performed on single crystals of UO_2 to study the directional dependence of higher-order-multipole scattering from the uranium $O_{4,5}$ edges (90–110 eV). By comparing the experimental results with theoretical calculations the symmetry of the ground state is confirmed directly as the crystal-field (CF) Γ_5 triplet state within the $J = 4$ manifold. The results demonstrate that the directional dichroism of the NIXS spectra is sensitive to the CF strength and establish NIXS as a tool for probing CF interactions quantitatively.

DOI: 10.1103/PhysRevB.98.205108

I. INTRODUCTION

Whilst in low-energy x-ray spectroscopy the electric-dipole transitions prevail, the advent of high-energy synchrotron radiation provides an opportunity to explore also higher-order multipole transitions. These transitions are governed by different selection rules that are reaching other final states, offering complementary spectroscopic perspectives. This is especially useful because the different multipole transitions are often well-separated in energy from each other due to the electrostatic interactions in the final state. Furthermore, the bulk sensitivity of hard x rays offers a clear advantage over soft x rays and allows spectroscopy under extreme conditions as well as the study of samples, such as actinides, that must be encapsulated for safety reasons.

One particular high-energy technique is nonresonant inelastic x-ray scattering (NIXS), in which a photon-in (ν_i), photon-out (ν_f) process promotes a core electron to an unoccupied valence state. This is given by the transition $\ell^n + \nu_i \rightarrow \underline{c}\ell^{n+1} + \nu_f$, where ℓ^n represents a valence shell ℓ with n electrons, and $\underline{c}$ denotes a hole in the core state. Multipole moments k for the $c \rightarrow \ell$ transition are allowed by the triangle condition $|\ell - c| \leqslant k \leqslant \ell + c$ and the parity rule $\ell + c + k =$ even. Thus for $d \rightarrow f$ transitions, $k = 1$ (dipole), $k = 3$ (octupole), and $k = 5$ (triakontadipole) transitions are allowed. The relative contributions of the multipole moments depend on the magnitude of the momentum transfer $\mathbf{q}$. A high intensity of the $k = 3$ and 5 transitions compared to $k = 1$ is obtained by using a large $|\mathbf{q}|$ ($\sim$10 Å^{-1}), as achieved with hard x rays, typically $\sim$10 keV, at large scattering angles. NIXS yields new spectroscopic features, which have been well described theoretically and successfully compared to experiments without assuming realistic crystal-field (CF) potentials [1–13]. In this paper, we investigate the effect of a finite CF potential.

NIXS has no intermediate state so that the interpretation is as straightforward as for x-ray absorption spectroscopy (XAS) [14]. The momentum transfer $\mathbf{q}$ in NIXS takes the place of the light polarization ε in XAS. Importantly, XAS is primarily governed by dipole transitions, which cannot distinguish between spherical symmetry and cubic symmetry, since the transferred angular momentum $k = 1$ branches to a single representation with no angular dependence. However, in cubic symmetry the transitions of angular momenta $k = 3$ and 5 branch to several different representations, each with its own distinct angular dependence. This anisotropy means that measurements with $\hat{\mathbf{q}} = \mathbf{q}/|\mathbf{q}|$ along different crystal directions can give a nonzero difference signal (directional dichroism) that provides information on the asphericity of the electronic ground state. NIXS measurements done by Gordon *et al.* [5] at the Mn $M_{2,3}$ edge ($3p \rightarrow 3d$) on a cubic single crystal of MnO already revealed different spectra for $\hat{\mathbf{q}}$ along the [111] and [100] directions.

Here we demonstrate the power of the $\mathbf{q}$ direction dependence of NIXS in a single crystal of uranium dioxide. UO_2 has been studied extensively for more than 50 years. We know that this material has two $5f$ electrons with a Γ_5 triplet ground state. This information has primarily come from neutron scattering—the CF splitting was determined in 1989 [15] and the excitation spectrum was reported conclusively in 2011 [16], after pioneering work 50 years ago [17]. Extensive theory on the interactions in UO_2 [18] and more recently studies using self-consistent DFT + U calculations

*Corresponding author: gerrit.vanderlaan@diamond.ac.uk
†Present address: ALBA Synchrotron Light Source, E-08290 Cerdanyola del Vallès, Barcelona, Spain.

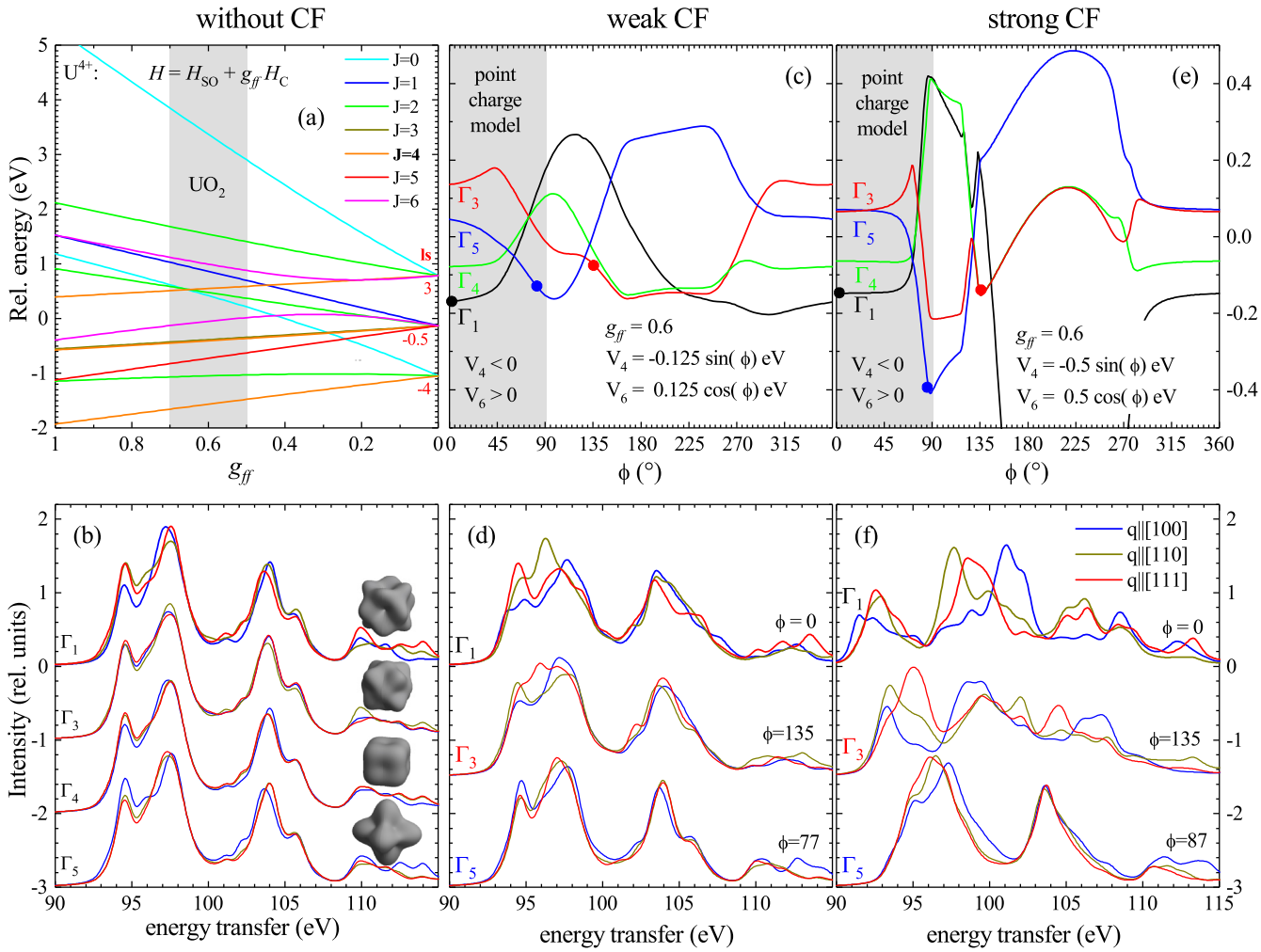

FIG. 1. (a) Energy level diagram of the J levels for the configuration U^{4+} $5f^2$ without CF as a function of the Slater reduction factor g_{ff}. The gray-shaded region marks the applicable range for UO_2. (b) Calculated NIXS spectra of the four cubic eigenstates as constructed by symmetry for pure $J = 4$ [see Eq. (1)] for $\hat{\mathbf{q}}\|[001]$ (blue), $\hat{\mathbf{q}}\|[011]$ (dark yellow), and $\hat{\mathbf{q}}\|[111]$ (red). The insets show the respective charge densities for two electrons. (c) and (e) Energy-level diagrams of CF states as a function of the ratio of the CF parameters $V_4 = -A \sin\phi$ and $V_6 = A \cos\phi$, expressed in terms of ϕ, for a weak and as strong CF scenario (see text). The colored dots mark selected Γ_1, Γ_3, and Γ_5 ground states used for the direction-dependent NIXS calculations in panels (d) and (f).

and a model Hamiltonian [19,20] have also been reported. Given this profound knowledge of the ground state of UO_2, we have performed NIXS experiments to test that the new technique gives the correct results for UO_2, establishing the importance of the directional dependence of the NIXS spectra. Comparing experiments with a series of calculations shows unambiguously that the Γ_5 triplet is indeed the ground state. In addition, by extending such calculations to cover different CF strengths, we show that the technique is sensitive to the CF strength and the admixture of the wave functions.

II. EXPERIMENT

The NIXS experiment has been performed using the RIXS spectrometer on beamline ID20 at the European Synchrotron Radiation Facility in Grenoble, France [21]. The beam generated by three consecutive undulators was monochromatized using a channel-cut Si(311) coupled to a Si(111) double-crystal momochromator and horizontally focused by a Rh-coated mirror. A set of five spherically bent Si(660) analyzer crystals with a 1-m bending radius, horizontal scattering geometry, and vertical Rowland circles provided an energy resolution of ~0.65 eV at a final photon energy of $E_f = 9.690\,02$ keV and an intensity of 7×10^{13} photons/s for a 25-μrad vertical divergence of the undulator radiation. The Bragg angle of the analyzers was fixed at 87.5°. The analyzers were placed at scattering angles $2\theta = 100$, 110, 120, 130, and 140°. The scattered intensity was recorded by a MAXIPIX fast readout, photon-counting position-sensitive detector, achieving up to a 1.4-kHz frame rate with a 290-μs readout dead time, with a pixel size of 55 μm and a detection geometry of 256 × 256 pixels.

For the measurements we used two UO_2 single crystals, originally cut and polished by Walt Ellis at Los Alamos National Laboratory [22], with (001) and (111) surfaces, respectively, and fully described in Ref. [23]. The samples were aligned with the [001] and [111] surface normal parallel to the averaged momentum transfer that points towards 150° for

elastic scattering. The [011] direction was realized by rotating the [001] crystal accordingly. For data analysis, only data collected in the highest analyzer at 140° were used because here the momentum transfer is largest ($|\mathbf{q}| = 9.1$ Å^{-1}). The corresponding momentum transfer at elastic scattering points towards 160°; i.e., there is an offset of 10° between the respective crystallographic directions and $\mathbf{q}$ which has been taken into account in the data analysis.

The (e^{-1}) penetration length for x rays of 10 keV into UO_2 is ~5 μm, so this probe is sensitive to the top ~2.5 μm. This is far greater than any surface effects extend, so NIXS may truly be considered as a bulk probe. Data have been collected at room temperature by scanning the incident energy $E_i = E_f + \hbar\omega_i$ at fixed final energy, covering the energy-transfer interval corresponding to the uranium $O_{4,5}$ ($5d \rightarrow 5f$) absorption edges. The obtained results were consistent with earlier measured isotropic spectra of UO_2 [6,7].

III. CALCULATION

Simulations were performed using the full-multiplet code QUANTY [24] that includes Coulomb and spin-orbit interactions. The calculations are based on an ionic approach for the U^{4+} $5f^2$ configuration. In intermediate coupling, the total momentum J is a good quantum number and the ground state is $J = 4$ [Fig. 1(a)]. The atomic parameters were calculated using Cowan's atomic multiplet code [25] and the Slater integrals for Coulomb interaction were reduced to account for intra-atomic relaxation effects [26]. Figure 1(a) shows the energy-level diagram for U^{4+} $5f^2$ as a function of the Slater reduction factor g_{ff}. This reduction factor was adjusted such that the energy distributions of the calculated isotropic and experimental pseudoisotropic spectra matched. The latter was constructed from the weighted sum of the measured directions; the calculated spectrum is the sum of the diagonal elements of the scattering tensor (see the Appendix). Here no CF has been taken into account. For the $5f$–$5f$ and $5d$–$5f$ Coulomb interactions we used reduction factors g_{ff} and g_{fc} equal to 0.6, and the $5f$ spin-orbit coupling was not reduced. The reduction factors change the overall shape of the isotropic spectra but have no direct influence on the $\mathbf{q}$-direction dependence of spectra. For the simulations we used a value of $|\mathbf{q}|$ slightly larger than that given by the experimental scattering condition because the radial part of the wave functions is based on the atomic values. A variation of $|\mathbf{q}|$ changes slightly the ratio of the multipole contributions [7,12]. Finally, a Gaussian and a Lorentzian broadening of 0.65 and 0.6 eV full width at half maximum, respectively, accounted for instrumental resolution and lifetime effects.

If the Coulomb interaction is much larger than the spin-orbit interaction (LS-coupling limit) the ground state is $^3H_4$, but a finite spin-orbit interaction gives intermixing with the $^1G_4$ and $^3F_4$ states. In the Stevens approximation [27], which ignores intermixing with $J \neq 4$ levels, the ground state is a mixture of different $J = 4$ levels (see Table I in the Appendix). The CF acts only on J and can be written for the cubic point-group O_h in the $|J_z\rangle$ basis set. Defining the $\hat{J}_x$ operator for the phase relation as positive, the ninefold $J = 4$ level splits up into

$$
\begin{aligned}
|\Gamma_1\rangle &= 0.456\ |-4\rangle + 0.456\ |+4\rangle + 0.764\ |0\rangle, \\
|\Gamma_3\rangle &= \begin{cases} 0.541\ |-4\rangle + 0.541\ |+4\rangle - 0.644\ |0\rangle, \\ 0.707\ |-2\rangle + 0.707\ |+2\rangle, \end{cases} \\
|\Gamma_4\rangle &= \begin{cases} 0.707\ |-4\rangle - 0.707\ |+4\rangle, \\ 0.935\ |\mp 1\rangle + 0.355\ |\pm 3\rangle, \end{cases} \\
|\Gamma_5\rangle &= \begin{cases} 0.707\ |-2\rangle - 0.707\ |+2\rangle, \\ 0.355\ |\mp 1\rangle - 0.935\ |\pm 3\rangle. \end{cases}
\end{aligned} \tag{1}
$$

We calculated the NIXS spectra of these eigenstates for different $\hat{\mathbf{q}}$ directions [Fig. 1(b)]. The respective two-electron charge densities are displayed as insets. Note that these are the *calculations without CF* since the states were constructed as given above, i.e., in the absence of a finite CF. The spectra with $\hat{\mathbf{q}}\|[001]$ (blue) and $\hat{\mathbf{q}}\|[111]$ (red) in Fig. 1(b) show the strongest direction dependence, especially at ~95, 97, and 105 eV. Particularly, the Γ_5 and Γ_1 states show an opposite direction dependence at these energies. Hence it should be possible to identify a Γ_5 state, which is the CF ground state expected from a previous inelastic neutron scattering study [15].

IV. RESULTS

Experimental results are shown in Fig. 2(a). While it is tempting to assign the main peak splitting in the spectra as O_5 ($5d_{5/2} \rightarrow 5f$) and O_4 ($5d_{3/2} \rightarrow 5f$), caution should be exercised. In XAS and electron-energy-loss spectroscopy (EELS) the dipole transitions ($k = 1$) result in a broad peak around 110 eV accompanied by a small prepeak at ~105 eV with an energy splitting that is mainly governed by the $5d$–$5f$ exchange interaction [26]. In NIXS, on the other hand, the observed energy splitting between the (95–97) and 105 eV peaks is primarily due to the $5d$ core spin-orbit splitting [10]. The peak at 95 eV arises mainly from $k = 5$ transitions, whereas the peaks at 97 and 105 eV arise from both $k = 3$ and $k = 5$ transitions. According to the spin-orbit sum rule [9] a change in angular momentum quantum number J changes the intensity ratio of the spin-orbit-split peaks. Here instead we are looking for differences in the angular dependence.

For the actinide $O_{4,5}$, as well as the rare-earth $N_{4,5}$, edges the dipole transitions are strongly broadened due to super-Coster-Kronig decay to continuum states [26,28]. However, compared to the dipole transitions the higher-order multipole transitions, which excite to final states with larger spin and orbital momenta, are shifted towards lower energy due to the strong $5f$–$5d$ exchange interaction [10]. As a result, higher-order multipole transitions have a substantially narrower linewidth with a broadening primarily determined by the core-hole lifetime.

Figure 2(a) shows the experimental NIXS spectra for the same momentum transfer and directions as in Fig. 1(b), i.e., for $\hat{\mathbf{q}}\|[001]$ (blue), $\hat{\mathbf{q}}\|[011]$ (dark yellow), and $\hat{\mathbf{q}}\|[111]$ (red). As can be seen in Fig. 1(d), Γ_5 is the only ground state to give the "up-down" nature of the first dichroic signal in the energy range of 94–97 eV, as shown in Fig. 2(b).

TABLE I. Weights (squared contributions) of respective LSJ states to the ground-state wave functions for the three different cases: the Stevens approximation, a weak CF, and a strong CF. In the case of the Stevens approximation, the J admixture is identical for all CF states. For the weak and strong cases the ground-state wave functions are chosen as in Figs. 1(d) and 1(f) of the main text.

LSJ states	Stevens	Γ_5 Weak CF	Γ_5 Strong CF	Γ_3 Weak CF	Γ_3 Strong CF	Γ_1 Weak CF	Γ_1 Strong CF
$^3H_4$	0.860	0.864	0.718	0.881	0.531	0.823	0.583
$^3H_5$	0	0.002	0.010	0.011	0.105	0	0
$^3H_6$	0	0	0.008	0.026	0.106	0.050	0.132
$^3F_2$	0	0	0.047	0.013	0.101	0	0
$^3F_3$	0	0	0.040	0	0	0	0
$^3F_4$	0.012	0.010	0.022	0.044	0.156	0.116	0.270
$^1G_4$	0.128	0.122	0.143	0.020	0	0.006	0
$^1D_2$	0	0	0.002	0	0	0	0
$^1I_6$	0	0	0.006	0.004	0	0.003	0.003
$^3P_0$	0	0	0	0	0	0.002	0.010
$^3P_1$	0	0	0	0	0	0	0
$^3P_2$	0	0	0.004	0.002	0	0	0
$^1S_0$	0	0	0	0	0	0	0.002

So far we have ignored the intermixing with $J \neq 4$ levels, although J mixing is expected in actinide compounds. The question is, to what extent does this mixing affect the interpretation of the NIXS data. We therefore calculated NIXS spectra for different CF scenarios. Figures 1(c) and 1(e) show the energy-level diagrams for a weak and a strong CF potential as a function of the ratio of the CF parameters V_4 and V_6 [15,29]. Their ratio is expressed in terms of ϕ with $V_4 = -A \sin\phi$ and $V_6 = A \cos\phi$, with $A = 0.125$ and 0.5 (in eV) for the weak and the strong CF case, respectively. In the gray-shaded range ($\phi < 90°$), $V_4 < 0$ and $V_6 > 0$ according to a point-charge model [30]. The wild ϕ dependence of the energy levels in the strong CF case is due to the large LSJ intermixing, which in the weak CF case is much more behaved. It turns out that Γ_4 can never be the ground state, and neither can Γ_3 within the point-charge model, in agreement with Lea, Leask, and Wolf [30]. For the remaining states the direction-dependent NIXS spectra have been calculated.

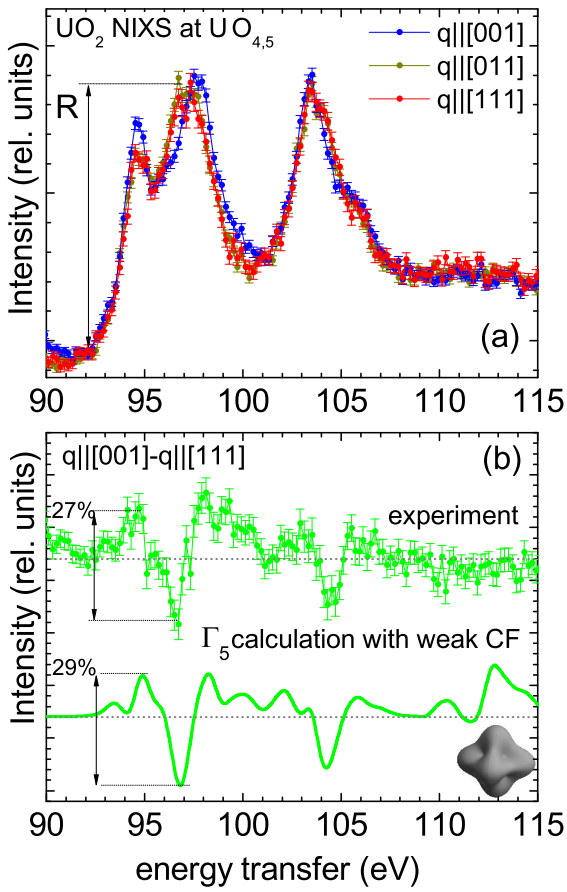

FIG. 2. (a) NIXS data of UO_2 measured at 300 K. (b) Measured difference spectra (directional dichroism) of the two directions $\hat{\mathbf{q}}\|[001] - \hat{\mathbf{q}}\|[111]$ and the corresponding calculation for the weak CF case with the Γ_5 ground state (green lines), see text.

The NIXS spectra for selected CF parameters that produce Γ_1 (black dots), Γ_3 (red dots), and Γ_5 (blue dots) ground states are shown in Figs. 1(d) and 1(f). The scheme of Amoretti *et al.* [15] is realized in the weak CF scenario for $\phi = 77°$ and that of Rahman and Runciman [31] is realized in the strong CF case for $\phi = 87°$. For the NIXS calculation the reduction factors and linewidths are kept unchanged because modifying g_{ff} and g_{fc} does not improve agreement between calculated and measured pseudoisotropic spectra (see the Appendix). Especially the spectra of the Γ_1 and Γ_3 ground states change substantially with increasing LSJ intermixing, the Γ_5 less so. The mixing factors of the respective ground states are listed in Table I of the Appendix.

Comparison of the calculated CF ground state and data shows that Γ_1 and Γ_3 still have to be excluded as ground states, both in the weak and the strong CF scenarios. Γ_5 of the strong CF case still shows some resemblance to the measured spectra, e.g., the high-energy tail of the peak at ~98 eV still shows stronger scattering for $\hat{\mathbf{q}}\|[001]$ than for the two other directions (blue over red and dark yellow). However, the direction dependence at 95 eV is much better reproduced for the weak CF with a Γ_5 ground state. The latter actually describes the data very well. Figure 2(b) shows the excellent agreement between the measured and the calculated direction dependence by comparing the difference plots of the [001] and [111] directions. Even the size of the observed

dichroism agrees very well with the calculated one, as shown by the relative values of 27% and 29%. These numbers refer to the difference of the two directions at energies indicated in Fig. 2(b), relative to the peak height R [as defined in Fig. 2(a)].

We should emphasize that the theoretical dichroism appearing above 110 eV is difficult to observe experimentally because all states at higher-energy transfers, i.e., in the energy range of the dipole transition ($\hbar\omega > 108$ eV) [7,12], appear strongly broadened due to interaction with continuum states. This increase in lifetime broadening is not captured in the calculations [13].

V. DISCUSSION AND CONCLUSIONS

The exceptional agreement observed in Fig. 2(b) between experiment and theory shows that the symmetry is unambiguously that of the Γ_5 triplet in the weak CF scenario, i.e., within the $J = 4$ manifold. Other CF symmetries as well as the strong CF scenario can be unambiguously excluded.

Although CF transitions are observed in almost all rare-earth materials with inelastic neutron scattering [32], this is not the case in actinide and some Ce heavy-fermion materials [33]. For ionic materials, such as UO_2, CF transitions are indeed observed [15], but for intermetallic systems the conduction electrons interact with the $5f$ states to cause a severe broadening of the CF transitions. Also XAS and EELS, in which dipole transitions dominate, suffer from severe broadening for intermetallic uranium systems [26,34,35], so that the excitonic effect of the higher multipole transitions in NIXS offers a great advantage. For UO_2, which is cubic, the dipole ($k = 1$) spectrum cannot provide information on the anisotropy of the charge distribution, so that an examination of higher-order multipole transitions is essential. Hence the NIXS technique represents an alternative method compared to neutron scattering and x-ray absorption spectroscopy to determine the symmetry of the ground state in such materials. Indeed, such a study has already been published on *tetragonal* URu_2Si_2 [12], and the ground-state symmetry was determined but without considering the effect of a strong versus a weak CF. The inelastic neutron scattering, however, shows a number of broad CF transitions and is thus unable to establish the ground state [36,37].

Our results open up an entire new world of higher multipole moment transitions. We have corrected the idea that cubic symmetry is optically isotropic. Higher multipole moments allow us to fit a set of different spectra, instead of a single spectrum as for dipole transitions. NIXS can also observe dipole-forbidden d-d and f-f transitions. Multipole transitions, which will become readily available from high-energy x-ray sources, will lead to new ways of doing spectroscopy. Among the applications will be areas like astrophysics, where high-energy radiation provides a glimpse of the constituting matter of distant constellations. NIXS is able to probe a broad class of materials. The unique combination of penetrating power and element specificity makes it an excellent candidate for identifying explosives in concealed environments. NIXS needs only small sample volumes, the photon-matter interaction is relatively strong, compared to, e.g., the neutron-matter interaction. This enables us to perform NIXS on very small volume samples, thin films, buried interfaces, and nano-objects, in addition to separate grains and facets of crystalline materials.

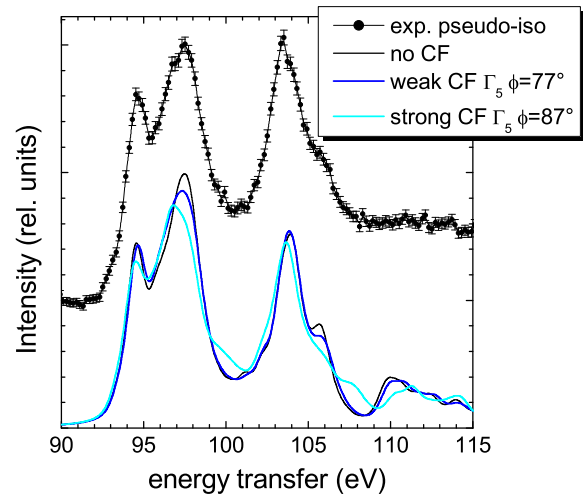

FIG. 3. Experimental pseudoisotropic spectrum of UO_2 as constructed from the single-crystalline data (black dots) and calculated NIXS spectra (lines), without considering a CF (black line), with a Γ_5 ground state in a weak CF (blue line), and with a Γ_5 ground state in a strong CF (cyan).

ACKNOWLEDGMENTS

We acknowledge beamtime on beamline ID20 at the European Synchrotron Radiation Facility (ESRF) in Grenoble, France, under Proposal No. HC-743. M.S. and A.S. benefited from the financial support of the Deutsche Forschungsgemeinschaft (DFG) under Grant No. SE-1441-5-1.

APPENDIX: CALCULATION OF THE ISOTROPIC SPECTRA

The isotropic spectra have been calculated from the trace of the scattering tensor, which corresponds to an integration over all $\hat{\mathbf{q}}$ directions. The Gaussian linewidth is determined by the instrumental resolution, so that only the lifetime (Lorentzian linewidth), Slater reduction factors g_{ff} and g_{fc}, and $5f$ spin-orbit interaction are adjustable parameters. All calculations in Fig. 3 are performed with the parameters as given in the main text.

The pseudo-isotropic spectrum is a linear combination of the three measured directions that yields an isotropic spectrum for $k = 1$ and 3, in good agreement with previously measured isotropic spectra of UO_2. [6,7] The prefactors depend on the point group. For the present O_h case: $I_{\mathrm{Iso}} = [40I(\hat{\mathbf{q}}\|[100]) + 32I(\hat{\mathbf{q}}\|[110]) + 27I(\hat{\mathbf{q}}\|[111])]/99$ considering $k = 1$ and 3. For $k = 5$ transitions we did not measure enough directions to provide the true isotropic spectrum, but the error is negligible when comparing calculations of the true and pseudoisotropic spectra.

[1] J. A. Soininen, A. L. Ankudinov, and J. J. Rehr, Inelastic scattering from core electrons: A multiple scattering approach, Phys. Rev. B **72**, 045136 (2005).

[2] B. C. Larson, W. Ku, J. Z. Tischler, C.-C. Lee, O. D. Restrepo, A. G. Eguiluz, P. Zschack, and K. D. Finkelstein, Nonresonant Inelastic X-Ray Scattering and Energy-Resolved Wannier Function Investigation of d-d Excitations in NiO and CoO, Phys. Rev. Lett. **99**, 026401 (2007).

[3] M. W. Haverkort, A. Tanaka, L. H. Tjeng, and G. A. Sawatzky, Nonresonant Inelastic X-Ray Scattering Involving Excitonic Excitations: The Examples of NiO and CoO, Phys. Rev. Lett. **99**, 257401 (2007).

[4] R. A. Gordon, G. T. Seidler, T. T. Fister, M. W. Haverkort, G. A. Sawatzky, A. Tanaka, and T. K. Sham, High multipole transitions in NIXS: Valence and hybridization in $4f$ systems, Europhys. Lett. **81**, 26004 (2008).

[5] R. A. Gordon, M. W. Haverkort, S. Sen Gupta, and G. A. Sawatzky, Orientation-dependent x-ray Raman scattering from cubic crystals: Natural linear dichroism in MnO and CeO_2, J. Phys.: Conf. Ser. **190**, 012047 (2009).

[6] J. A. Bradley, S. Sen Gupta, G. T. Seidler, K. T. Moore, M. W. Haverkort, G. A. Sawatzky, S. D. Conradson, D. L. Clark, S. A. Kozimor, and K. S. Boland, Probing electronic correlations in actinide materials using multipolar transitions, Phys. Rev. B **81**, 193104 (2010).

[7] R. Caciuffo, G. van der Laan, L. Simonelli, T. Vitova, C. Mazzoli, M. A. Denecke, and G. H. Lander, Uranium $5d$–$5f$ electric-multipole transitions probed by nonresonant inelastic x-ray scattering, Phys. Rev. B **81**, 195104 (2010).

[8] J. A. Bradley, K. T. Moore, G. van der Laan, J. P. Bradley, and R. A. Gordon, Core and shallow-core d- to f-shell excitations in rare-earth metals, Phys. Rev. B **84**, 205105 (2011).

[9] G. van der Laan, Spin-Orbit Sum Rule for Electric Multipole Transitions in Nonresonant Inelastic X-Ray Scattering, Phys. Rev. Lett. **108**, 077401 (2012).

[10] G. van der Laan, Nonresonant inelastic x-ray scattering from actinides and rare earths, Phys. Rev. B **86**, 035138 (2012).

[11] T. Willers, F. Strigari, N. Hiraoka, Y. Q. Cai, M. W. Haverkort, K.-D. Tsuei, Y. F. Liao, S. Seiro, C. Geibel, F. Steglich, L. H. Tjeng, and A. Severing, Determining the In-Plane Orientation of the Ground-State Orbital of $CeCu_2Si_2$, Phys. Rev. Lett. **109**, 046401 (2012).

[12] M. Sundermann, M. W. Haverkort, S. Agrestini, A. Al-Zein, M. M. Sala, Y. Huang, M. Golden, A. de Visser, P. Thalmeier, L. H. Tjeng, and A. Severing, Direct bulk-sensitive probe of $5f$ symmetry in URu_2Si_2, Proc. Natl. Acad. Sci. USA **113**, 13989 (2016).

[13] M. Sundermann, H. Yavaş, K. Chen, D. J. Kim, Z. Fisk, D. Kasinathan, M. W. Haverkort, P. Thalmeier, A. Severing, and L. H. Tjeng, $4f$ Crystal Field Ground State of the Strongly Correlated Topological Insulator SmB_6, Phys. Rev. Lett. **120**, 016402 (2018).

[14] G. van der Laan and A. I. Figueroa, X-ray magnetic circular dichroism—A versatile tool to study magnetism, Coord. Chem. Rev. **277-278**, 95 (2014).

[15] G. Amoretti, A. Blaise, R. Caciuffo, J. M. Fournier, M. T. Hutchings, R. Osborn, and A. D. Taylor, $5f$-electron states in uranium dioxide investigated using high-resolution neutron spectroscopy, Phys. Rev. B **40**, 1856 (1989).

[16] R. Caciuffo, P. Santini, S. Carretta, G. Amoretti, A. Hiess, N. Magnani, L.-P. Regnault, and G. H. Lander, Multipolar, magnetic, and vibrational lattice dynamics in the low-temperature phase of uranium dioxide, Phys. Rev. B **84**, 104409 (2011).

[17] R. A. Cowley and G. Dolling, Magnetic excitations in uranium dioxide, Phys. Rev. **167**, 464 (1968).

[18] P. Santini, S. Carretta, G. Amoretti, R. Caciuffo, N. Magnani, and G. H. Lander, Multipolar interactions in f-electron systems: The paradigm of actinide dioxides, Rev. Mod. Phys. **81**, 807 (2009).

[19] F. Zhou and V. Ozoliņš, Crystal field and magnetic structure of UO_2, Phys. Rev. B **83**, 085106 (2011).

[20] F. Zhou and V. Ozoliņš, Self-consistent density functional calculations of the crystal field levels in lanthanide and actinide dioxides, Phys. Rev. B **85**, 075124 (2012).

[21] M. Moretti Sala, K. Martel, C. Henriquet, A. Al Zein, L. Simonelli, C. Sahle, H. Gonzalez, M.-C. Lagier, C. Ponchut, S. Huotari, R. Verbeni, M. Krisch, and G. Monaco, A high-energy-resolution resonant inelastic x-ray scattering spectrometer at ID20 of the European Synchrotron Radiation Facility, J. Synchrotron Radiat. **25**, 580 (2018).

[22] T. N. Taylor and W. P. Ellis, Distorted surface oxygen structure on UO_2(100), Surf. Sci. **107**, 249 (1981).

[23] G. M. Watson, D. Gibbs, G. H. Lander, B. D. Gaulin, L. E. Berman, H. Matzke, and W. P. Ellis, Resonant x-ray scattering studies of the magnetic structure near the surface of an antiferromagnet, Phys. Rev. B **61**, 8966 (2000).

[24] M. W. Haverkort, *Quanty* for core level spectroscopy—Excitons, resonances and band excitations in time and frequency domain, J. Phys.: Conf. Ser. **712**, 012001 (2016).

[25] R. D. Cowan, *The Theory of Atomic Structure and Spectra* (University of California, Berkeley, 1981).

[26] K. T. Moore and G. van der Laan, Nature of the $5f$ states in actinide metals, Rev. Mod. Phys. **81**, 235 (2009).

[27] K. W. H. Stevens, Matrix elements and operator equivalents connected with the magnetic properties of rare earth ions, Proc. Phys. Soc. A **65**, 209 (1952).

[28] J. Terry, R. K. Schulze, J. D. Farr, T. Zocco, K. Heinzelmann, E. Rotenberg, D. K. Shuh, G. van der Laan, D. A. Arena, and J. G. Tobin, $5f$ Resonant photoemission from plutonium, Surf. Sci. **499**, L141 (2002).

[29] N. Magnani, P. Santini, G. Amoretti, and R. Caciuffo, Perturbative approach to J mixing in f-electron systems: Application to actinide dioxides, Phys. Rev. B **71**, 054405 (2005).

[30] K. R. Lea, M. J. M. Leask, and W. P. Wolf, The raising of angular momentum degeneracy of f-electron terms by cubic crystal fields, J. Phys. Chem. Solids **23**, 1381 (1962).

[31] H.U. Rahman and W.A. Runciman, A crystal field calculation in uranium dioxide, J. Phys. Chem. Solids **27**, 1833 (1966).

[32] P. Fulde and M. Loewenhaupt, Magnetic excitations in crystal-field split $4f$ systems, Adv. Phys. **34**, 589 (1985).

[33] K. A. Gschneidner, Jr., L. Eyring, G. H. Lander, and G. R. Choppin (eds.), *Handbook on the Physics and Chemistry of Rare Earths*, Vol. 19 (North-Holland, Amsterdam, 1994), Chap. 130 by E. Holland-Moritz and G. H. Lander and Chap. 131 by G. Aeppli and C. Broholm.

[34] J. R. Jeffries, K. T. Moore, N. P. Butch, and M. B. Maple, Degree of $5f$ electron localization in URu_2Si_2: Electron energy-loss spectroscopy and spin-orbit sum rule analysis, Phys. Rev. B **82**, 033103 (2010).

[35] L. A. Wray, J. Denlinger, S.-W. Huang, H. He, N. P. Butch, M. B. Maple, Z. Hussain, and Y.-D. Chuang, Spectroscopic Determination of the Atomic f-Electron Symmetry Underlying Hidden Order in URu_2Si_2, Phys. Rev. Lett. **114**, 236401 (2015).

[36] P. Santini, G. Amoretti, R. Caciuffo, F. Bourdarot, and B. Fåk, Field-Dependent Energy Scales in URu_2Si_2, Phys. Rev. Lett. **85**, 654 (2000).

[37] J.-G. Park, K. A. McEwen, and M. J. Bull, High-energy magnetic excitations of URu_2Si_2, Phys. Rev. B **66**, 094502 (2002).